ACS OMEGA

http://pubs.acs.org/journal/acsodf

Article

Cytotoxicity and Antibacterial Potentials of Mixed Ligand Cu(II) and Zn(II) Complexes: A Combined Experimental and Computational Study

Mamaru Bitew Alem,* Tegene Desalegn,* Tadewos Damena, Enyew Alemayehu Bayle, Moses O. Koobotse, Kennedy J. Ngwira, Japheth O. Ombito, Matshediso Zachariah, and Taye B. Demissie*

Cite This: *ACS Omega* 2023, 8, 13421−13434

Read Online

ACCESS | Metrics & More | Article Recommendations | Supporting Information

ABSTRACT: $[Cu(C_{15}H_9O_4)(C_{12}H_8N_2)O_2C_2H_3]\cdot 3H_2O$ (**1**) and $[Zn(C_{15}H_9O_4)(C_{12}H_8N_2)]O_2C_2H_3$ (**2**) have been synthesized and characterized by ultraviolet−visible (UV−vis) spectroscopy, Fourier transform infrared (FTIR) spectroscopy, mass spectrometry, thermogravimetric analysis/differential thermal analysis (TGA/DTA), X-ray diffraction (XRD), scanning electron microscopy−energy-dispersive X-ray spectroscopy (SEM-EDX), and molar conductance, and supported by density functional theory (DFT) and time-dependent DFT (TD-DFT) calculations. Square pyramidal and tetrahedral geometries are proposed for Cu(II) and Zn(II) complexes, respectively, and the XRD patterns showed the polycrystalline nature of the complexes. Furthermore, *in vitro* cytotoxic activity of the complexes was evaluated against the human breast cancer cell line (MCF-7). A Cu(II) centered complex with an IC_{50} value of 4.09 μM was more effective than the Zn(II) centered complex and positive control, cisplatin, which displayed IC_{50} values of 75.78 and 18.62 μM, respectively. In addition, the newly synthesized complexes experienced the innate antioxidant nature of the metal centers for scavenging the DPPH free radical (up to 81% at 400 ppm). The biological significance of the metal complexes was inferred from the highest occupied molecular orbital−lowest unoccupied molecular orbital (HOMO−LUMO) energy band gap, which was found to be 2.784 and 3.333 eV, respectively for **1** and **2**, compared to the ligands, 1,10-phenathroline (4.755 eV) and chrysin (4.403 eV). Moreover, the molecular docking simulations against estrogen receptor alpha (ERα; PDB: 5GS4) were strongly associated with the *in vitro* biological activity results (E_B and K_i are −8.35 kcal/mol and 0.76 μM for **1**, −7.52 kcal/mol and 3.07 μM for **2**, and −6.32 kcal/mol and 23.42 μM for cisplatin). However, more research on *in vivo* cytotoxicity is suggested to confirm the promising cytotoxicity results.

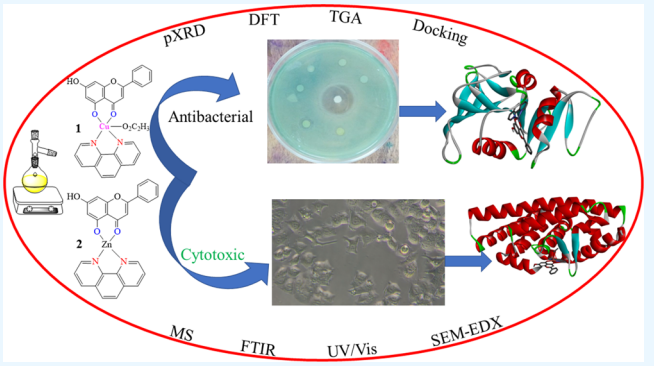

INTRODUCTION

The synthesis and use of transition metal complexes for medical- and health-related applications have gained momentum in recent years.[1] Transition metal complexes offer a rich platform for being used as therapeutic agents[2] ranging from antimicrobial and anti-inflammatory to anti-proliferative and enzyme inhibitory activities.[3] Their unique electronic and stereochemical properties, molecular geometries, ligand exchange, redox, catalytic, and photophysical reactions are among the major reasons for the convergence of attention toward the compounds' both therapeutic and diagnostic roles.[1,4] These unique properties give them the potential to interact and react with biomolecules in unique ways and by distinct mechanisms of action.[4,5] Copper(II) and zinc(II) are endogenous metal ions with high antimicrobial and antioxidant activities which are promising features to be used as metallodrugs.[6] On the other hand, research reports indicate that the nature of the organic ligand of these metal complexes is likely responsible for their pharmacological activity.[7] The important clinical role of metal coordination compounds of biologically active ligands has seen a lot of progress in their biological applications in recent years.[8]

Flavonoids are a large class of biologically active polyphenols with important biological properties. These include antidiabetic,[9] antibacterial,[10,11] anti-inflammatory,[12] cardioprotec-

Received: February 11, 2023
Accepted: March 20, 2023
Published: March 29, 2023

tive,[13] anticancer,[14] antiaging,[15] neuroprotective/antioxidant,[11,14,16] antiproliferative[11,17] and antiestrogenic[18] properties. In this regard, flavonoid-based metal complexes with higher antioxidant, anti-inflammatory, and tumor cell cytotoxicity activities of naringin−Cu(II) complex, $[Cu(Naringin)\text{-}(CH_3OH)_2]^+$, have been reported.[19] Cytotoxicity and DNA binding studies of copper(II) and zinc(II) complexes of flavonoids (Quercitrin, Myricitrin, and Rutin) were reported to exhibit an intercalative mode of DNA binding, nuclease, and DNAse activity with the metal complexes.[20] Similarly, higher antioxidant activity/free radical scavenging activity of Zn(II)-Butien (66%) than that of Butien (19%) alone has been reported,[6] indicating that metal complexes have greater biological activity than ligands alone. In our previous study,[21] 16 biologically active flavonoids were screened for their druglikeness, percent intestinal absorption, pharmacokinetics, and toxicity profiles. Among the studied flavonoids, chrysin was selected for its druglike molecular nature and less toxicity profiles. Chrysin (5,7-dihydroxyflavone) is among the biologically active bidentate flavonoid family ligands. Its homoleptic metal complexes were reported together with their anticancer,[22] inhibiting xanthine oxidase,[23] antioxidant,[24,25] cytotoxic,[26] and antibacterial activities. However, heteroleptic Cu(II) and Zn(II) complexes of chrysin and 1,10-phenathroline ligands as antibacterial and anticancer agents have never been reported.

In our previous work, we reported the synthesis, antibacterial, and cytotoxicity profile of Cu(II) complexes using 1,10-phenathroline and the drugs metformin and ciprofloxacin,[27] in which we achieved a promising cytotoxicity profile of Cu(II)-mixed drug complexes against MCF-7 cell lines. Inspired by the previous findings, we designed two other new complexes of Cu(II) and Zn(II) using 1,10-phenathroline and a biologically active ligand chrysin (Figure 1).

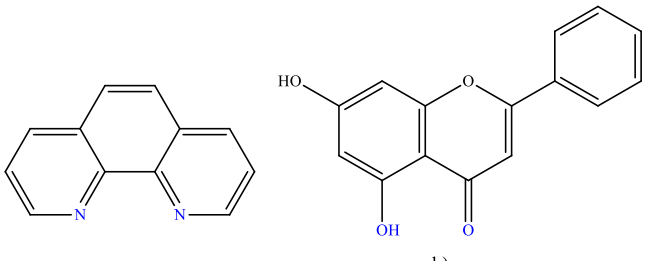

Figure 1. Structure and potential chelation sites of the ligands: (a) 1,10-phenanthroline and (b) chrysin.

The design of the research comprising the ligand screening, synthesis, characterization, and biological activity of the resulting metal complexes is presented in Figure 2.

EXPERIMENTAL SECTION

MATERIALS AND METHODS

Chrysin, ascorbic acid, and 2,2-diphenyl-1-picrylhydrazyl (DPPH) were purchased from Sigma Aldrich (Burlington, MA, USA) after *in silico* screening of bidentate biologically active flavonoids, while 1,10-phentahroline was purchased from BDH chemical Ltd. (England). $Cu(O_2C_2H_3)_2{\cdot}H_2O$, $Zn(O_2C_2H_3)_2{\cdot}2H_2O$, dimethyl sulfoxide (DMSO), and dimethylformamide (DMF) were purchased from Loba Chemie Pvt. Ltd. (India). Triethylamine (TEA), $NaHCO_3$, Mueller Hinton agar, methanol (MeOH), and diethyl ether were purchased from Alpha Chemika (India). All chemicals and reagents were of high purity and were used as received.

Thin layer chromatography (MERCK Silica gel 60 F254) together with UV Cabinet (UV−vis lamp at 254 and 365 nm) was used to monitor the progress of the chemical reactions. The melting points of the complexes were determined using the digital melting point (Hanchen digital auto melting point apparatus: model 934). UV−vis spectral data collected on an SM-1600 spectrophotometer from 200−800 nm were used to study the type of electronic shifts of the ligands before and after complexation. Molar conductance of the synthesized metal complexes was recorded at room temperature in DMSO having 1.0×10^{-3} M concentration using an electrical conductometer (AD8000). The vibrational frequencies of the ligands and corresponding metal complexes were recorded using FTIR (Perkin-Elmer BX spectrometer, Shimadzu Corporation, Japan) from 4000 to 400 cm^{-1} in a KBr pellet. The thermogravimetric/differential thermal analyses (TGA/DTA, DTG-60H SHIMADZU thermal analyzer) were used to record the thermal behavior of the reported complexes from 25−800 °C with a heating rate of 10 °C/min under a nitrogen atmosphere (20 mL/min). A high-resolution mass spectrometer (Waters-LCT-Premier mass spectrometer) using 2 ng/μL of sample concentration with a capillary voltage of 2500 V, at a desolvation temperature of 250 °C using nitrogen gas at 250 L/h, Bruker APEX II CCD area detector diffractometer, with graphite monochromated Mo K3 radiation (50 kV, 30 mA) and temperature of measurement at 173(2) K coupled with APEX 2 data collection software was used to obtain the spectra.[27] Scanning electron microscopy−energy-dispersive X-ray spectroscopy (SEM−EDX) measurements were performed with a Joel JSM-6500F instrument (Joel, Tokyo, Japan). X-ray diffraction (XRD-7000, Shimadzu Co., Japan) was used to determine the nature of the synthesized metal complexes. The diffraction was recorded with 2θ = 10 to 80 using CuKα (λ = 1.5406 Å) radiation operated at 40 kV and 30 mA, whereas the average crystalline sizes of the complexes were calculated according to the Debye−Scherrer equation.[28] The interplanar spacing (d), Miller indices (hkl), and lattice parameters (a, b, c, α, β and γ) were estimated using *QUALX2.0*.[29]

Synthesis. *Synthesis of Cu(II) and Zn(II) Mixed Ligand Complexes.* Heteroleptic metal complexes **1** and **2** employing chrysin with a co-ligand 1,10-phenathroline were synthesized using previously reported procedure[23] with minor modifications. For Cu(II) mixed ligand complex **1**, 1 mmol of chrysin (0.254 g) was added to a mixture of 20 mL of methanol−ethanol solution (1:3) in the presence of a deprotonating agent, 1 mmol NaOH, and stirred for 20 min, resulting in a clear yellow solution to which 1 mmol of $Cu(O_2C_2H_3)_2{\cdot}H_2O$ (0.199 g) was added slowly. The resulting blue−green solution was stirred for 20 min; then, 1 mmol of methanolic solution of 1,10-phenanthroline (0.198 g) was added slowly followed by 140 μL (1 mmol) of triethylamine. Then, the resulting green−brown solution was refluxed at 60 °C for 6 h as the progress of the reaction was monitored with TLC. Finally, diethyl ether was added to the obtained green−brown solution, which was then stored in a refrigerator at 4 °C for two weeks. Green−brown powders were collected from the filtrate after two weeks. The same procedure was employed for the synthesis of Zn(II) mixed ligand complex **2** using 1 mmol of $Zn(O_2C_2H_3)_2{\cdot}2H_2O$ (0.219 g) and 8 h of reflux to obtain a

https://doi.org/10.1021/acsomega.3c00916
ACS Omega 2023, 8, 13421−13434

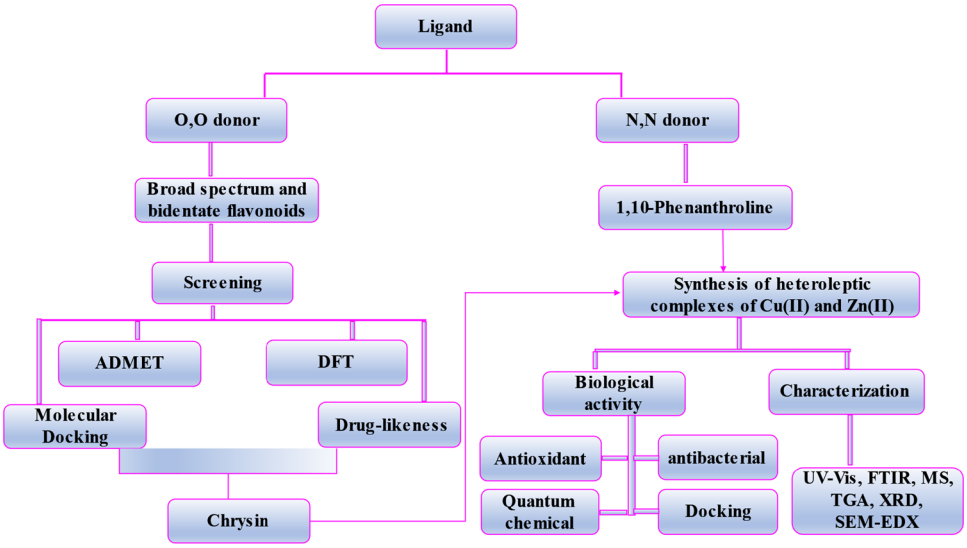

Figure 2. Diagrammatic representations of the research design.

Scheme 1. Schematic Representations of 1,10-Phenathroline−Chrysin Mixed Ligand Metal Complexes

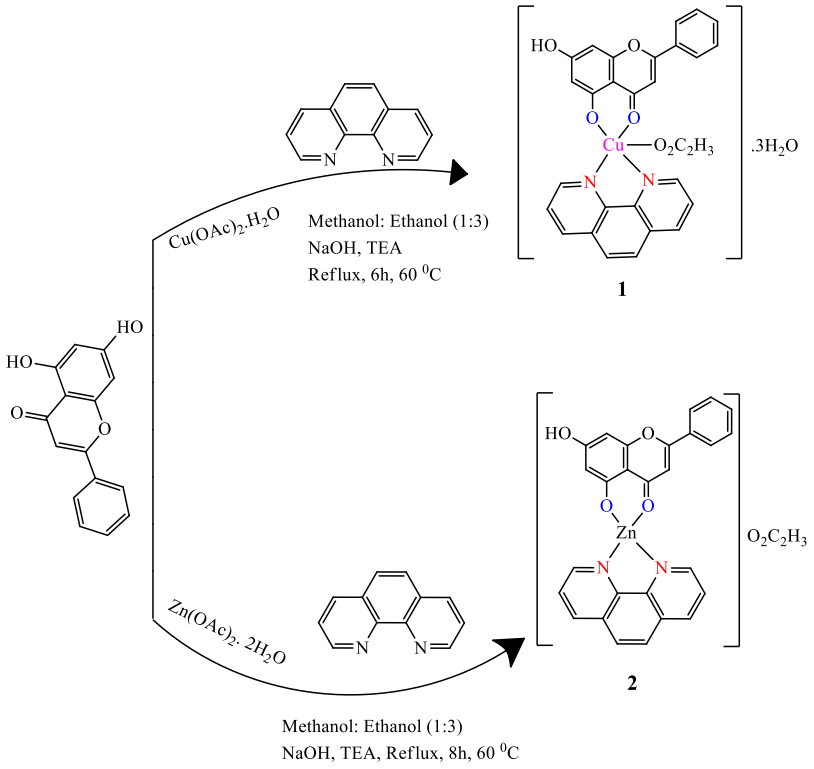

light-yellow powder. The proposed structures of the reported metal complexes and their schematic representations are presented in Scheme 1.

***In Vitro* Cytotoxicity Assay.** *In vitro* cytotoxic activities of the synthesized metal complexes were tested on the human breast cancer cell line (MCF-7). The MCF-7 cell line was a generous gift from Associate Professor Claire Perks (University of Bristol, United Kingdom) and was originally obtained from the European Collection of Authenticated Cell (ECACC) (Porton Down, Wiltshire, UK). Detailed cell culture conditions and procedures for the cytotoxicity assay were reported in our previous work.[27]

Antibacterial Activity. The *in vitro* antibacterial activities of the metal complexes were evaluated against the Gram-positive bacteria (*Escherichia coli* (ATCC25922) and *Pseudomonas aeruginosa* (ATCC27853)) and gram-negative bacteria (*Staphylococcus aureus* (ATCC25923) and *Streptococcus pyogenes* (ATCC19615)) by using the disk diffusion method in Mueller Hinton-Agar (MHA) medium. Ciprofloxacin was used as a positive control.[30] Known concentrations (500 and 1000 μM) of the metal complexes were prepared in DMSO. Ciprofloxacin (500 μM) in DMSO was used as a positive control, whereas DMSO was used as a negative control and no activity was found. The obtained results were presented in triplicates as a mean ± SD.[27]

https://doi.org/10.1021/acsomega.3c00916
ACS Omega 2023, 8, 13421−13434

Table 1. Physicochemical Properties of the Synthesized Metal complexes

compound	color	state	mass (% yield)	m.p (°C)	conductivity (Ω^{-1} cm^2 mol^{-1}, 25 °C)
1	green−brown	powder	0.303 g (49.672)	205	27.56
2	light-yellow	powder	0.113 g (20.324)	218	51.80

Antioxidant Activity Evaluation Using DPPH Radical Scavenging Activity. The capability of the synthesized metal complexes (**1** and **2**) as free radical scavengers was evaluated by conducting DPPH radicals and comparing the results with ascorbic acid as a standard antioxidant available. As previously described,[27] the solution of DPPH in methanol (400 ppm) was prepared and 1.0 mL of this solution was added to 3 mL of each of the test compounds. Different concentrations (25−400 ppm) of the test compounds (chrysin, **1**, and **2**) and the control, ascorbic acid, were prepared. The reaction mixture was vortexed for 10 s and allowed to stand at room temperature for 30 min in a dark. The associated fade in the color of DPPH was observed and the absorbance of the resulting mixture was recorded at 517 nm.[31] The percentage of DPPH radical scavenging activity was calculated using equation 1.

$$\%\text{DPPH radical scavenging activity} = \frac{A_c - A_s}{A_c} \times 100\% \quad (1)$$

where A_c is the absorbance of the control and A_s is the absorbance of a test sample.

Computational Details. Geometry optimizations of the structures were performed using density functional theory (DFT) employing the B3LYP[32] hybrid functional together with the 6−311++G(d, p) basis set[33] for atoms of the ligand (H, C, N, O, and Cl), whereas the Los Alamos National Laboratory 2-double-zeta (LanL2DZ) pseudopotential was employed for the metal atoms (Cu and Zn)[34] to account for relativistic effects. The nonbonding interactions during the calculations were considered using Grimme's dispersion correction[35] because good computational and experimental agreements were obtained for this combination of methods as we previously reported.[21,36] The time-dependent DFT (TD-DFT) and vibrational frequency calculations were performed at the same level of theory. The optimized geometries were confirmed to be a real minimum without the negative imaginary vibrational frequencies. Quantum chemical descriptors and band gap energies of the synthesized metal complexes were calculated from Frontier Molecular Orbitals (FMOs). Chemcraft (version 1.8) was employed to visualize the highest occupied molecular orbital (HOMO) and the lowest unoccupied molecular orbital (LUMO) and calculate the band gap energy. The Eigen values of the FMOs were used to calculate the quantum chemical descriptors: electronegativity ($\chi = -1/2(E_{HOMO} + E_{LUMO})$), electrochemical potential ($\mu = 1/2(E_{HOMO} + E_{LUMO}) = -\chi$), global chemical hardness ($\eta = 1/2(E_{LUMO} - E_{HOMO})$), global softness ($\sigma = 1/2\eta$), global electrophilic index ($\omega = \mu^2/2\eta$), and nucleophilic index ($Nu = 1/\omega$). These quantum chemical descriptors were used to relate the structures with the experimentally obtained biological activities of the complexes as reported in previous studies.[27,37,38]

Molecular Docking Studies. In order to predict the interaction of the synthesized compounds (**1** and **2**) with the binding sites of estrogen receptor alpha (ERα; PDB:5GS4)[39] and dihydrofolate reductase (PDB:2w9h) (DHR) which are proteins of MCF-7 and *S. aureus*, respectively, a molecular docking study was performed. Prior to the molecular docking study, the geometries of the metal complexes were optimized using the B3LYP-GD3/6−311++G(d,p)/LanL2DZ method and converted to PDB files using GaussView. The molecular docking study was performed using the AutoDock 4.2.6[40] following the same protocols as previously reported in our studies.[21,27,41] Briefly, the PDB files for ERα and DHR were downloaded from the respective Protein Data Bank. To remove the co-crystallized substrate and water molecules, MGL 1.5.6 software was used. Polar hydrogens were added together with the Kollman charges. Nonpolar hydrogen atoms were merged and Gasteiger partial atomic charges were assigned to the molecules. Standard docking parameters for all the light and metal atoms were used. The grid box was constructed using 120, 120, and 120 pointing in the *x*, *y*, and *z* dimensions, respectively, with a grid point spacing of 0.375 Å. The center grid box was set at −12.055, −10.491, and 5.964 Å for the *x*, *y*, and *z* centers, respectively. The Lamarckian genetic algorithm (LGA) program[42] with an adaptive whole method search in the AutoDock was selected and set at 100, which generated 100 different conformations for each of the molecules.[43] The conformers with the lowest binding free energies were used for the visualization of the interactions between the active amino acids and the molecules using the Discovery Studio software. The molecular docking results were compared with the positive controls cisplatin and ciprofloxacin.[27]

RESULTS AND DISCUSSION

Characterization of Heteroleptic Cu(II) and Zn(II) complexes. *Physicochemical Properties.* The synthesized metal complexes (**1** and **2**) were subjected to the solubility test using solvents of different polarities. It was observed that complexes **1** and **2** were soluble in DMF and DMSO, respectively. The percentage yields, melting points, color, and state of the synthesized metal complexes are presented in Table 1.

Molar conductance analysis was conducted to ascertain the electrolytic and nonelectrolytic nature of the synthesized metal complexes. The low value of the molar conductance of compound **1** (27.56 Ω^{-1} cm^2 mol^{-1}) suggested its nonelectrolytic nature, while the relatively higher value of the molar conductance of compound **2** (51.80 Ω^{-1} cm^2 mol^{-1}) suggested its electrolytic nature[44] (Table 1). By combining the molar conductance data with other spectroscopic and spectrometric techniques (*vide infra*), the geometries were predicted to be square pyramidal for complex **1** ($[Cu(C_{12}H_8N_2)(C_{15}H_9O_4)(C_2H_3O_2)]\cdot 3H_2O$) and tetrahedral for complex **2** ($[Zn(C_{12}H_8N_2)(C_{15}H_9O_4)]C_2H_3O_2$).

FTIR Analysis. The IR spectrum (experimental/B3LYP calculated) of chrysin showed broad bands at 3430/3698, 1640/1608, and 2930/3123 cm^{-1} due to ν_{-OH}, $\nu_{-C=O}$, and ν_{-C-H}, respectively (Figure 3). The large vibrational frequency difference for the −OH group between the experimental and B3LYP calculated could be attributed to the presence of intermolecular hydrogen bonding in the experimental measurement.[45] The reduction in the ν_{-OH} intensity of chrysin from

https://doi.org/10.1021/acsomega.3c00916
ACS Omega 2023, 8, 13421−13434

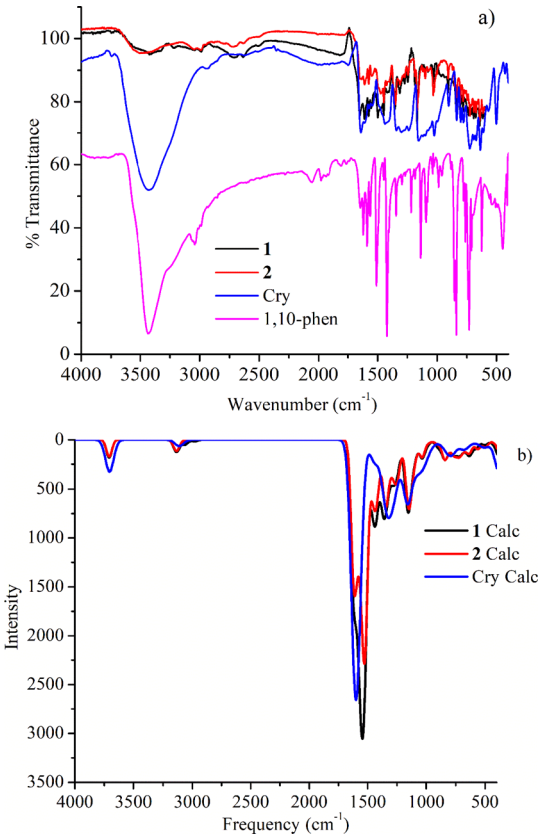

Figure 3. Experimental (a) and calculated (b) FTIR spectra of the ligands (1,10-phen, Cry) and their metal complexes (**1** and **2**).

52% transmittance to 94 and 95% for complexes **1** and **2**, respectively, confirms the coordination of chrysin to the metal centers in a monoprotonated fashion. Moreover, the vibrational frequency of $\nu_{-C=O}$ shifts to a higher frequency of 1648 and 1656 cm^{-1} for **1** and **2**, respectively, suggesting that the metals bind chrysin via the oxygen atom of the carbonyl group of the flavonoid ring which is consistent with previously reported studies.[24] Furthermore, from the IR spectrum, the stretching vibrational bands of the 1,10-phenanthroline monohydrate ligand for $\nu_{-C=C}$ (1622/1592 cm^{-1}) and $\nu_{-C=N}$ (1586/1550 cm^{-1}) functional groups were shifted to lower frequencies (1606/1608 cm^{-1}) and (1555/1512 cm^{-1}) for **1** and 1614/1611 cm^{-1} and (1546/1528 cm^{-1}) for **2** with a decrease in intensity. The stretching vibrational bands for ν_{-O-H} (3430 cm^{-1}) associated with the water of crystallization of 1,10-phenathroline are diminished following the metal−ligand coordination (Figure 3). The decrease in their intensity indicates the formation of a rigid and symmetric structure in the metal center.[46] Besides the observed vibration frequency shifts, the formation of metal−ligand bonds was confirmed by the appearance of new vibrational bands (experimental/calculated) at 687/734 and 645/586 cm^{-1} for **1** and 678/724 and 645/565 cm^{-1} for **2** which are associated with the formation of M−O and M−N bonds, respectively.

UV−vis/TD-DFT Analysis. The UV−visible spectrum of the ligands chrysin and 1,10-phenathroline was recorded in DMSO. The experimental and TD-DFT calculated results are shown in Figure 4. The absorption peaks (experimental/TD-DFT) at 267/261 and 320/325 nm, due to $\pi \rightarrow \pi^*$ transitions of the benzoyl system and the cinnamoyl system, respectively, were reported for chrysin. For 1,10-phenathroline free ligands

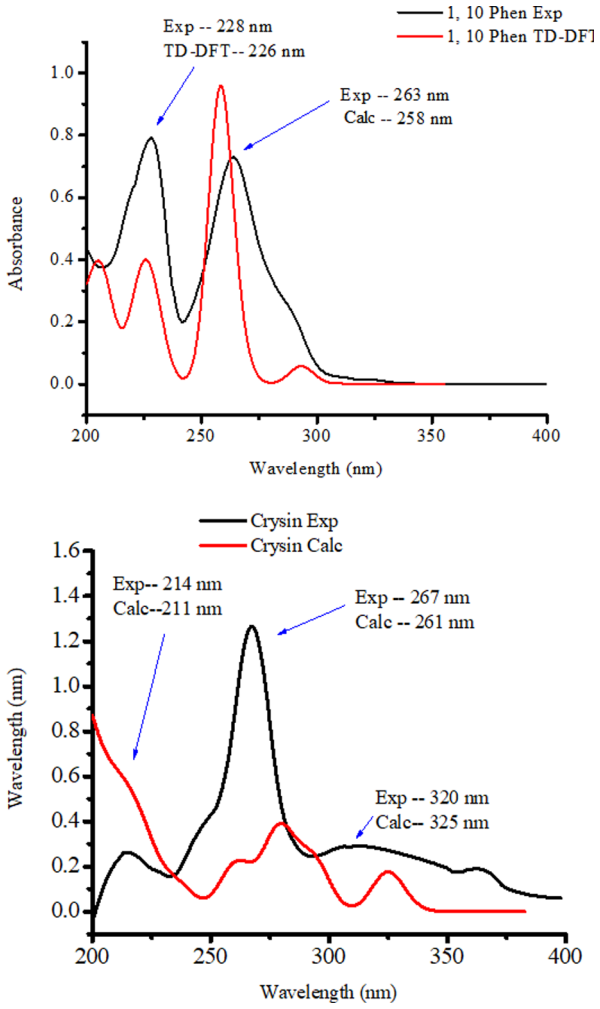

Figure 4. UV−vis and TD-DFT calculated absorption spectrum of the ligands (chrysin and 1,10-phenanthroline).

(experimental/TD-DFT), the absorption peaks at 228/226 and 263/258 nm due to n → π^* (C═N) and $\pi \rightarrow \pi^*$ (C═C) transitions, respectively, were reported.[27]

A bathochromic shift was observed for 1,10-phenathroline and chrysin at 276 and 272 nm for complexes **1** and **2**, respectively. The broad peak at 320/325 nm for chrysin was found to diminish. This might be due to the extension of the conjugated system with metal complexation. A new stronger absorption peak that appeared at 396 nm (25,252 cm^{-1}) for **1** (Figure 5) resulted from the formation of complexes between chrysin, 1,10-phenanthroline, and Cu(II) metal ion centers.[47]

The coordination of Cu(II) with chrysin in complex **1** caused a red shift of 9 and 76 nm, for the benzoyl and cinnamoyl part, respectively. This indicates that chelation brought enhanced conjugation to the cinnamoyl system of chrysin than to the benzoyl system. Thus, we reasonably concluded that the coordination of chrysin was via its carbonyl oxygen.[48] There was little red shift (6 and 2 nm) in complex **2**, which could be due to the predominant electron transfer raised from interligands, absence of d → d transition, and higher band gap energy in the Zn(II) complex as a result of d^{10} electron configuration.[49] Moreover, the absence of a peak above 400 nm for complex **2** could be due to nonexiting ligand-to-metal charge transfer bands in Zn(II) metal-centered complexes (Figure 6). However, the resulting changes in the electronic

https://doi.org/10.1021/acsomega.3c00916
ACS Omega 2023, 8, 13421−13434

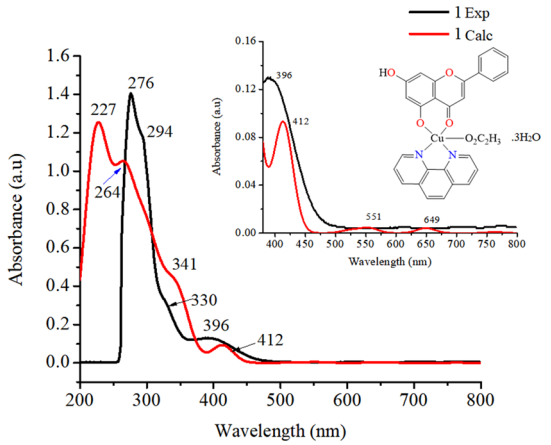

Figure 5. UV−vis (*black*) and TD-DFT (*red*) absorption spectra of complex **1**.

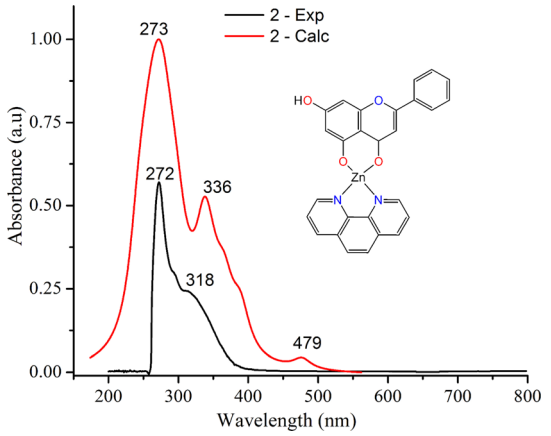

Figure 6. UV−vis (black) and TD-DFT (red) absorption spectra of complex **2**.

structure of the ligands upon complexation of the Zn(II) metal center are confirmed by the observed spectral pattern of complex **2**.

Mass Spectrometric Analysis. The mass spectra of the complexes were obtained, and it was observed that *m/z* values are in good agreement with their molecular formula mass, as presented in Figures S1, S2 of the Supporting Information. The mass spectra of complex **1** showed the molecular ion peak at *m/z* = 612.959 (found 609.090) attributed to the complex cation $[C_{29}H_{27}CuN_2O_9]^+$. A peak at *m/z* = 572.266 (found 573.040) was attributed to the coordination sphere, acetate ion, and a water molecule ($M^+ + H_2O + C_2H_3O_2$) $[C_{29}H_{22}CuN_2O_7]$, while a peak at *m/z* = 496.048 (found 496.050) corresponded to the chemical species in the coordination sphere ($M = [C_{27}H_{17}CuN_2O_4]^+$. The fragments for the coordinating ligands chrysin and 1,10-phenathroline in complex **1** were found to appear as peaks at 255.065 and 181.076, respectively. Complex **2** showed a molecular ion peak at *m/z* = 497.046 (found 497.050) corresponding to a Zn-centered coordination sphere cation $[C_{27}H_{17}N_2O_4Zn]^+$. Fragments associated with the coordinating ligands were observed as in complex **1**. The absence of a coordinating acetate ion in complex **2** could be due to its loss as a result of the operating cone voltage.[50]

Powder XRD Analysis. The powder X-ray diffraction (PXRD) spectra of **1** and **2** complexes were obtained for structural characterization. The XRD patterns of **1** and **2** mixed ligand complexes show diffraction peaks which indicate the polycrystalline phases of the synthesized complexes, as shown in Figure 7. The XRD pattern of the powders shows many diffraction peaks with different intensities in the range $2\theta = 5-30°$, indicating the polycrystalline phases (Figure 7).

The crystal system of Cu(II) mixed ligand complex (**1**) was found to be orthorhombic ($\alpha = \beta = \gamma = 90°$) with spacing group P21 and lattice parameters 14.574, 17.358, and 20.413 Å for *a*, *b*, and *c*, respectively. Complex **2** was found to be an orthorhombic crystal system with spacing group *Pnma* and lattice parameters 22.361, 10.350, and 7.826 Å for *a*, *b*, and *c*, respectively. Moreover, the average crystalline size of the complexes was calculated according to the Debye−Scherrer equation.[28] It was found that the average crystallite sizes of the complexes were 19.766 and 18.050 nm for **1** and **2**, respectively. The percent crystalline index of the complexes was calculated using eq 2.

$$\text{Crystalline Index (CI)} = \frac{A_c}{A_c + A_a} \times 100\% \quad (2)$$

where A_c is the area of crystalline and A_a is the area of the of amorphous part of the materials.

Accordingly, the synthesized mixed ligand complexes were found to show 27.208 and 40.914% crystallinity for **1** and **2**, respectively. Then, the number of dislocation lines per unit area of the crystal and the dislocation density ($\delta*$) of the complexes were calculated from its relation to the average crystallite size (D) of the complexes[51,52] using eq 3.

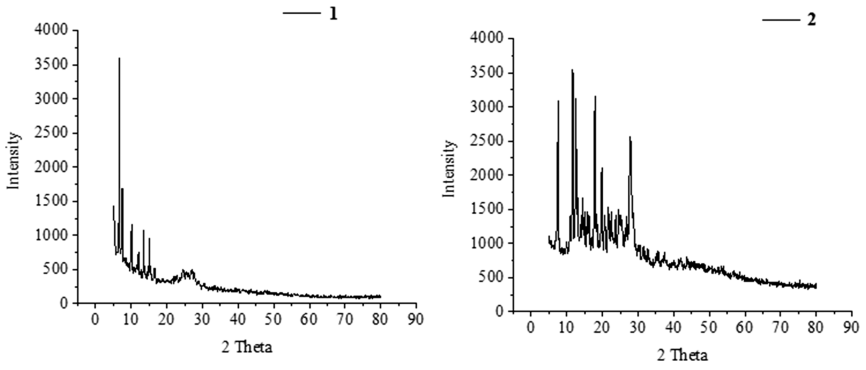

Figure 7. PXRD patterns for Cu(II)(**1**) and Zn(II) (**2**) mixed ligand complexes.

https://doi.org/10.1021/acsomega.3c00916
ACS Omega 2023, 8, 13421−13434

$$\text{Dislocation density } (\delta^*) = \frac{1}{D^2} \quad (3)$$

The calculated dislocation density values were found to be 2.559×10^{-3} and 3.069×10^{-3} nm^{-2} for complexes **55** and **56**, respectively, confirming a crystalline material with a relatively less dislocation density and less irregularity within the structure. Previous research work by El-Sonbati and coworkers reported dislocation density values ranging from 3.00×10^{-4}–2.10×10^{-3} nm^{-2} for Cu(II), Ni(II), Mn(II), and UO_2(II) mixed ligand polycrystalline complexes.[52]

Thermogravimetric Analysis. Thermal stability of the synthesized complexes (**1** and **2**) was identified based on thermogravimetric analysis having a temperature range from 25 to 800 °C (Figure 8). Complex **1** thermally decomposed into

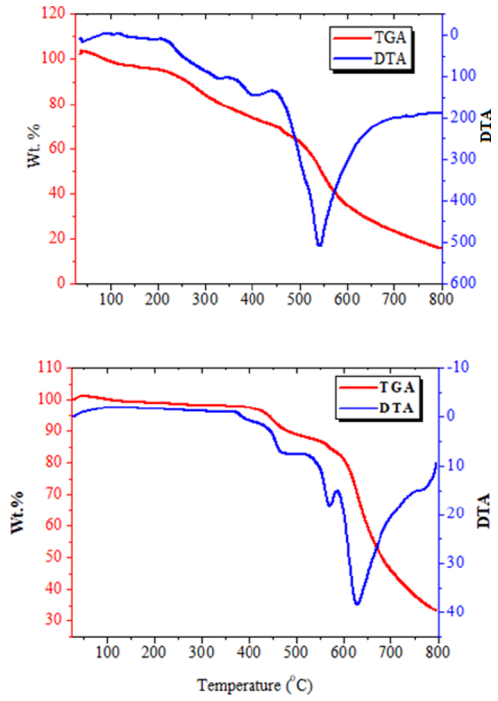

Figure 8. Graphical presentation of the TGA/DTA of complexes **1** (top) and **2** (bottom).

three main degradation steps. The first step suggested the loss of three lattice water molecules in the temperature range of 100–211 °C (DTG_{max} = 162 °C) having a weight loss of 8.81% (cald. 8.84%). The second step took place at the temperature range of 215–484 °C (DTG_{max} = 403 °C), which suggested the removal of the $C_{12}H_8N_2$ organic moiety having a weight loss of 29.47% (calcd. 29.49%). In the last step, the weight loss of 43.53% (calcd. 43.87%) at a temperature range 490–752 °C suggested the loss of the CHO_2 + $C_{15}H_{11}O_2$ organic moieties, leaving behind the residue of copper oxide as an end product (Table 2 and Figure 8).[53] Similar decomposition behavior was also observed for complex **2**, which also degraded in three decomposition steps and finally left with zinc oxide as the final product (Table 2).

SEM–EDX Analysis. The elemental composition of the reported complexes was obtained from EDX analysis (Figure 9). The SEM picture of the synthesized complexes shows agglomerated particles and the presence of nonuniform-sized small grains. The EDX spectrum of **1** showed characteristic signals associated with carbon, nitrogen, oxygen, and copper,

Table 2. Temperature Range Values for Decomposition and Corresponding Weight Loss Values

cpds	decomposition temp. (°C)	mass loss (%) obsd	mass loss (%) calcd.	interpretation
1	100–211	8.81	8.84	loss due to three lattice water molecules
	215–484	29.47	29.49	release of the $C_{12}H_8N_2$ organic moiety
	490–752	43.53	43.87	release of the CHO_2 + $C_{15}H_{11}O_2$ organic moieties
2	100–428	3.40	3.41	loss due to the hydroxyl group
	429–560	10.64	10.77	loss due to C_3H_3O groups organic moiety
	565–788	51.94	52.23	loss due to $C_3H_4N_2$ + $C_{15}H_9O_4$ organic moieties

confirming the formation of a CHCuNO, whereas the EDX spectrum of complex **2** was found to show characteristic signals associated with carbon, nitrogen, oxygen, and zinc, confirming the formation of a CHZnNO-type complex compound.[27]

Biological Studies. *In Vitro Cytotoxicity Assay.* Cell viability was evaluated on the MCF-7 cell line using the MTT assay with six variable concentrations of test compounds in triplicate, as depicted in Figure 10. For comparison, cisplatin was used as a positive control. At 3.125 μM concentration, the viability of MCF-7 cells was reduced to 67.36% by complex **1** compared to complex **2** (95.41%) and cisplatin (89.17%), demonstrating high cytotoxicity of complex **1** to the MCF-7 cells even at the lowest concentration.

The cytotoxicity of the synthesized complexes and the positive control strongly depend on concentration. Complex **1** (IC_{50} = 4.09 μM) displayed relatively a higher cytotoxicity than the positive control, cisplatin (IC_{50} = 18.62 μM), and complex **2** (IC_{50} = 75.78 μM), indicating that Cu(II) complexes of 1,10-phentharoline display promising cytotoxicity potentials against the MCF-7 cell line. The IC_{50} values of the synthesized complexes are comparable to those reported previously for mixed ligand copper(II) complexes named Casiopeina (IC_{50} values ranging from 2.2 to 103.7 μM) against the same cell line.[54,55] It has been reported that lower percentage cell viability is associated with higher cytotoxic potential of the test compound and that a test compound is considered cytotoxic if it reduces cell viability to less than 70%.[56] Hence, both the reported compounds (**1** and **2**) were cytotoxic at 25 μM with IC_{50} values in the range reported in previous studies.[27,54] In our previous work, a Cu(II) complex that shows cytotoxicity at 12.5 μM (cell viability = 15.19%) with IC_{50} value 4.29 μM was reported. Complex **1** was designed to contain a natural flavonoid chrysin and 1,10-phenathroline and demonstrated an improved cytotoxicity starting from 3.125 μM at which the cell viability decreased to 67.36%. This infers the potency of Cu(II) complexes as future cytotoxic agents. The change in the metal center of the two complexes, a Cu(II) centered (**1**) and Zn(II) centered (**2**), and the variations in the geometry of the complexes bring a considerable difference in the cytotoxicity of the complexes. Hence, complex **1** was found to demonstrate approximately 19-fold bioactivity over complex **2**, mainly due to differences in the geometry and metal center of the complexes.

Microscopic images provided in Figure 11a–d show the cell morphology of untreated MCF-7 cells and those treated with 50 μM of **1**, **2**, and cisplatin for 24 h. MCF-7 cells are characterized by their epithelial morphology with irregular and

https://doi.org/10.1021/acsomega.3c00916
ACS Omega 2023, 8, 13421–13434

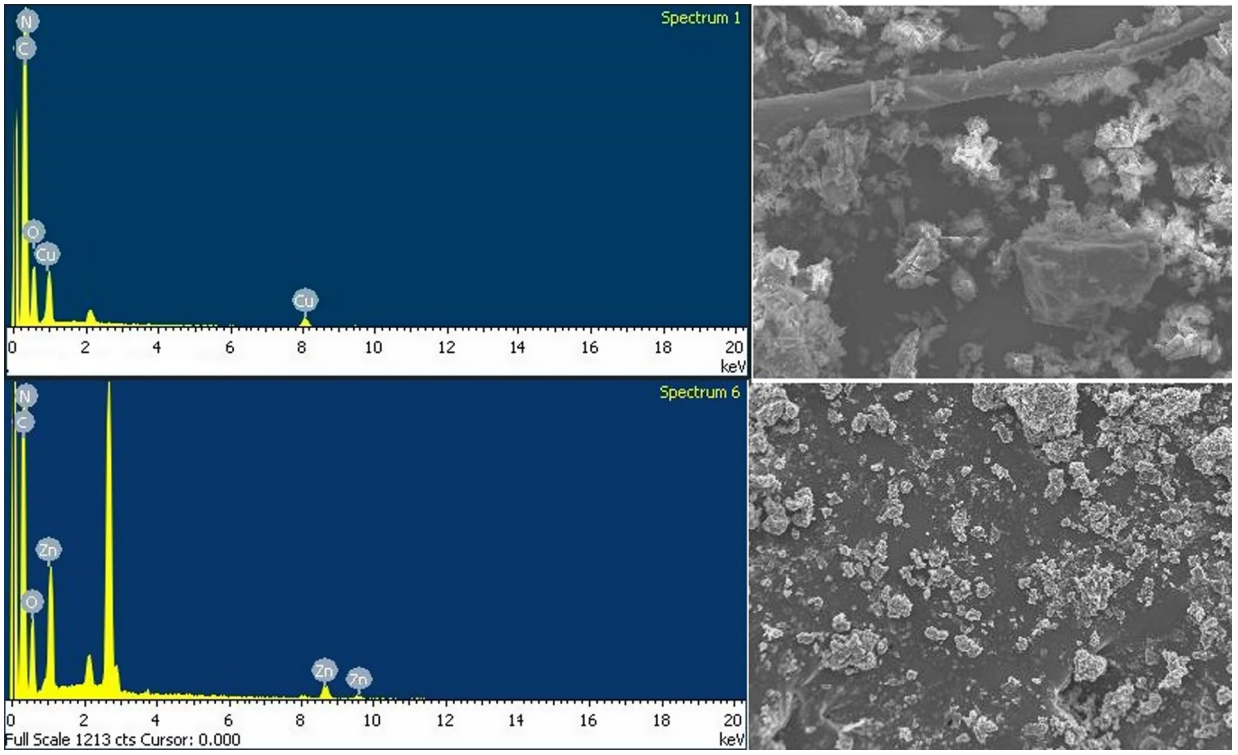

Figure 9. EDX (Left) and SEM (right) images of complexes **1** (top) and **2** (bottom).

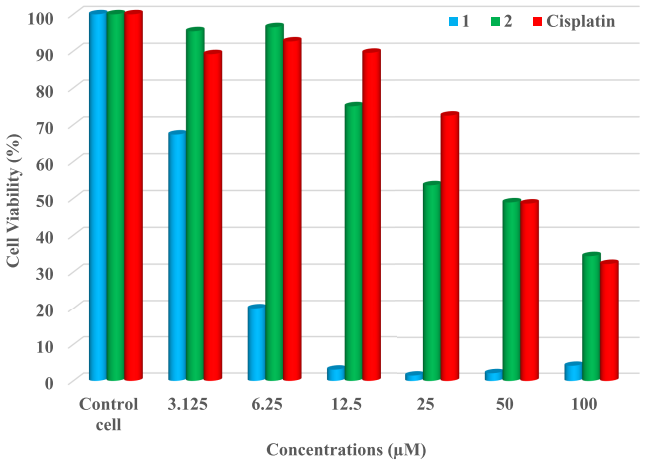

Figure 10. Cell viability of the MCF-7 cell line at different concentrations with respect to control cells.

polygonal cells,[57] as observed in untreated MCF-7 cells (Figure 11a). However, after treatment with 50 μM **of 1**, **2**, and cisplatin for 24 h, the cells displayed altered morphology and reduced cell density. This observation was more evident for complex **1**. Generally, the obtained microscopic and percent cell viability results demonstrated that the reported metal complexes are cytotoxic as reported for other metal complexes.[27,55,57]

Antibacterial Activity. The synthesized mixed ligand metal complexes (**1** and **2**) were tested against four bacterial strains (Gram-negative: *E. coli* and *P. aeruginosa*, and Gram-positive: *S. aureus* and *S. pyogenes*). The complexes were found to show potent antibacterial activity against both types of bacterial strains. The obtained results are presented in Figure 12 and Table S4. Among the mixed ligand complexes, a Cu(II) complex, **1** showed strong antibacterial activity at both 500 and 1000 μM concentrations against all bacterial strains, followed by **2**. Detailed antibacterial activity results demonstrated that complex **1** showed a preference for Gram-positive bacterial strains, *S. aureus* and *S. pyogenes* at both concentrations. The minimum inhibition zones (MIZ) are found to be 11.000 $\pm$ 0.236 and 11.333 $\pm$ 0.577 mm for **1** against *S. pyogenes* and *S. aureus at* 500 μM. On the other hand, complex **2** was found to show preferences against *E. coli* and *S. pyogenes*, and *E. coli* and *S. aureus*, respectively, at 500 and 1000 μM concentrations.

The percent activity indexes (%AI) of the synthesized complexes were calculated to correlate with the observed MIZ values.[58] The percent activity indexes of complex **1** against *E. coli*, *P. aeruginosa*, *S. aureus*, and *S. pyogenes* were found to be 42.3, 46.3, 44.6, and 49.3%, respectively. Those of complex **2** were found to be 40.3, 38.1, 37.8, and 39.9%, respectively, for *E. coli*, *P. aeruginosa*, *S. aureus*, and *S. pyogenes*. The results demonstrate that complex **1** has better antibacterial activity than complex **2**. The higher antibacterial activity of complex **1** may be due to the smaller band gap energy (2.784 eV) than complex **2** (3.333 eV).

Antioxidant Activity. The antioxidant activities of chrysin and its heteroleptic complexes (**1** and **2**) were compared with the standard antioxidant, ascorbic acid. The results are presented in Figure 13. The percent free radical scavenging activities demonstrated that the synthesized heteroleptic complexes have higher antioxidant activities than the free ligand chrysin, indicating that the synthesized metal complexes have better biological activities than the free ligand. The free radical scavenging activities follow the order AA > **2** > **1** > chrysin. The slightly higher antioxidant activity of complex **2** might be associated with the higher energy of the HOMO (E_{HOMO} = −6.036 eV) of the complex compared to that of complex **1** (E_{HOMO} = −5.966 eV). The enhanced antioxidant activities of the metal complexes than the free ligand are in line

https://doi.org/10.1021/acsomega.3c00916
ACS Omega 2023, 8, 13421−13434

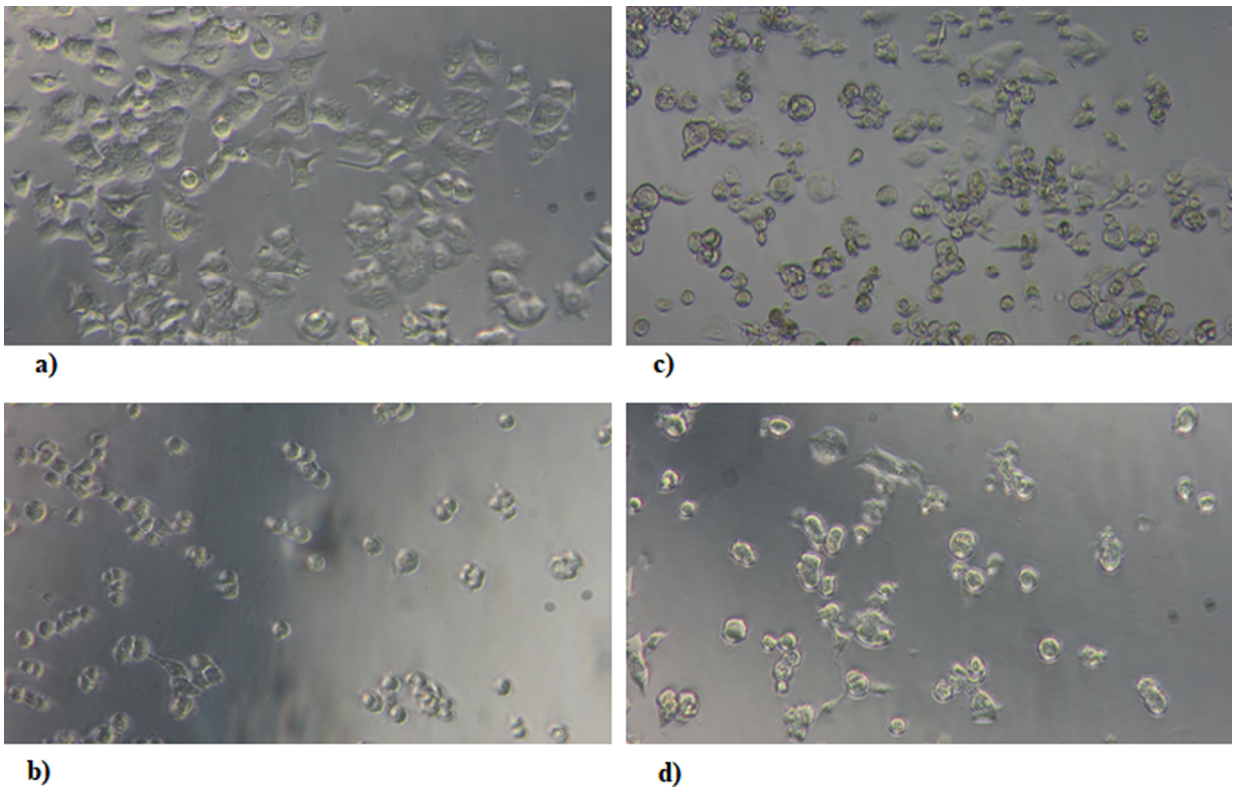

Figure 11. Photomicrographs of the cellular morphology of (a) untreated MCF-7 and the changes induced by complex **1** (b), cisplatin (c), and **2** (d) at 50 μM.

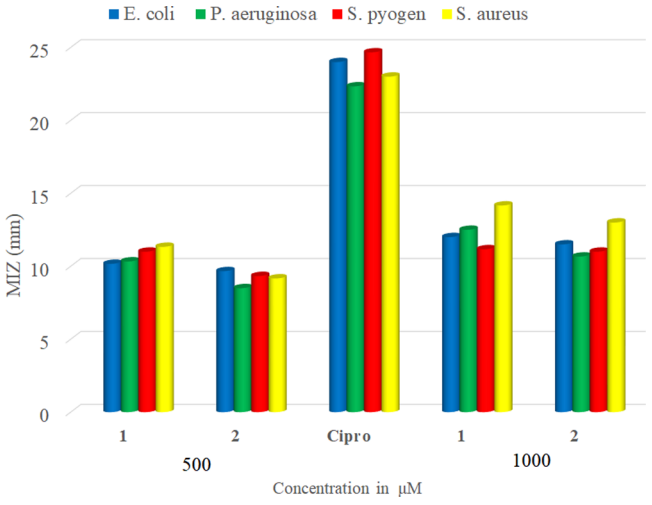

Figure 12. Antibacterial activity of 1,10-phenathroline and chrysin mixed ligand complexes (**1** and **2**).

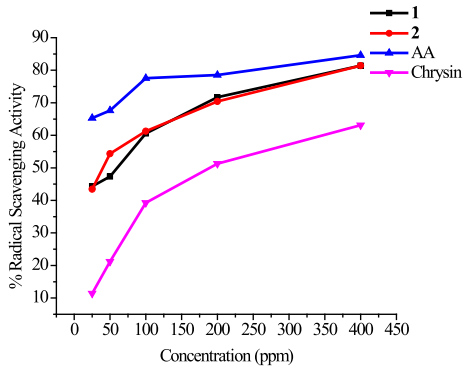

Figure 13. Antioxidant activity of the synthesized metal complexes (**1** and **2**) against DPPH radicals.

with the previously reported studies.[24,25,48] The antioxidant activities of our compounds exhibit the distinct characteristics of Zn and Cu-metal centers as radical scavengers.

Quantum Chemical Descriptors. The quantum chemical descriptors of the free ligands and the corresponding metal complexes are presented in Figure 14 and Table S2, whereas the wave function distributions are shown in Figures 15 and S3. In our previous study, we reported that the band gap energy (E_g) has a strong correlation with various biological activities: antibacterial, antioxidant, and cytotoxicity.[27,49,58] Moreover, band gap energy has been used as an important stability descriptor. A compound with large band gap energy is suggested to be stable and hard, whereas that with small band gap energy is less stable, giving the compound softness and enhanced biological importance.[38] In this work, the band gap energy of the ligands and the synthesized metal complexes were found to be 4.755, 4.403, 2.784, and 3.333 eV, respectively, for 1,10-phenanthroline, chrysin, **1**, and **2**. The decrease in the band gap energy of the complexes is correlated with the enhanced experimental antioxidant activities of the complexes than the free ligand chrysin (*vide supra*). The band gap energies of the metal complexes were found to be less than that of the ligands, inferring that the synthesized metal complexes are softer than the ligands (Figure 14 and Table S2). The observed decrease in the band gap energy of the metal complexes could be due to the presence of ligand-to-metal charge transfer (LMCT). According to the hard and soft acids and bases (HSAB) principle, soft acids prefer binding to

https://doi.org/10.1021/acsomega.3c00916
ACS Omega 2023, 8, 13421−13434

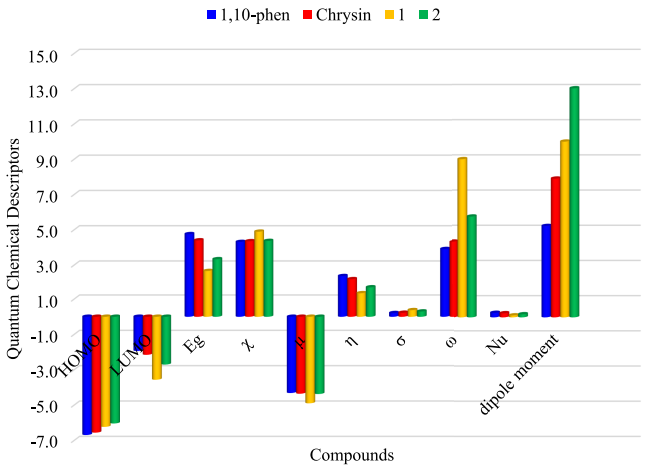

Figure 14. Graphical presentations of quantum chemical descriptors.

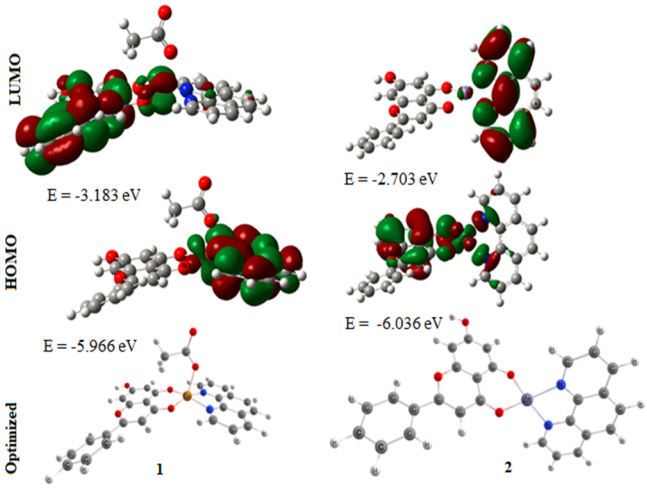

Figure 15. Optimized geometry, HOMO−LUMO, and Eigen values of Cu(II) (**1**) and Zn(II) (**2**) metal complexes.

soft bases to give covalent complexes, whereas hard acids prefer binding to hard bases to give ionic complexes.[38,59] The formation of a covalently bonded adduct through soft-soft molecular interaction preference to soft biological systems can weaken the functions of soft biological molecules: enzymes, DNA, cytoskeletal proteins, and other macromolecules, leading to malfunctioning cell processes and cytotoxicity.[59] Hence, the biological activity of a compound increases with increasing softness and decreasing hardness. In this study, the order of chemical hardness (η) was found to be 1,10-phen > chrysin > **2** > **1**, suggesting that complex **2** is more stable than **1**.

Chemical potential (μ) measures the tendency of an electron to escape from equilibrium, and it is directly proportional to the Gibbs free energy.[59] Also, it represents the ability of an electrophilic or nucleophilic species to undergo chemical change.[60] The chemical reactivity of a species increases with decrease in chemical potential. Thus, the chemical reactivity ranking of the synthesized complexes was found to be **1** > **2**, with 0.525 eV difference between **1** and **2**. Other important parameters computed for the ligands and the synthesized metal complexes were electrophilicity and nucleophilicity indexes. The electrophilicity index is associated with the ability of electron acceptance, whereas the nucleophilicity index is associated with electron-donating ability.[38] Quantitative information about the transition state energies involved in toxicant-protein adduct formation can be obtained from electrophilicity calculation. Thus, values for the electrophilicity index (ω) agree with the rate constant of the adduct formation and are directly related to toxicant strength.[60] The electrophilicity and nucleophilicity of the synthesized metal complexes were found to be 7.517 and 0.133 eV, and 5.729 and 0.175 eV, respectively, for **1** and **2**. This gives a chemical reactivity rank of **1** > **2** as an electrophile and vice versa as a nucleophile, in agreement with a previous study.[38] From computed electrophile index results, it can be inferred that complexes **1** and **2** could have better adduct formation. The dipole moment (in Debye) is a parameter related to the mobility of electrons. The higher the dipole moment of the compound, the higher is the active electron for the compound and the higher the biological activity.[61] The two complexes (**1** and **2**) showed large enhancement in the dipole moment relative to the ligands (Figure 14 and Table S3).

FMO Analysis. The electronic features of molecular structures can be calculated from FMOs: the HOMO and LUMO.[62] The B3LYP-calculated HOMO−LUMO distribution of the ligands and the corresponding metal complexes are presented in Figures 15 and S3. It is found that the spreading of isodensity shows the different trends in the HOMO and LUMO of the three complexes. In complex **1**, the isodensity is concentrated mainly on the 1,10-phenanthroline ring and the Cu-metal center, and the metal center and chrysin for the HOMO and LUMO, respectively. This inferred the presence of LMCT and d → d electronic transition. In complex **2**, the isodensity shows concentration on the Zn-metal center and chrysin for the HOMO and 1,10-phenanthroline for the LUMO, inferring the possible intraligand and metal-to-ligand charge transfer.

Molecular Docking Analysis. *Molecular Docking against Estrogen Receptor Alpha and S. aureus.* Estrogen receptor α (ERα) is one of the major clinical biomarkers used to subtype breast cancers. It plays an important role in the development and progression of dependent hormonal type breast cancer.[63] The interaction of the synthesized complexes (**1** and **2**) and the control cisplatin with estrogen receptor alpha (ERα; PDB:5GS4) residual amino acids, binding affinity (kcal/mol), and the inhibition constant (K_i) parameters are presented in Figure 16, Table 3, and Figure S4.

The binding affinity and inhibition constant of the studied compounds were found to be −8.35 and 0.76, −7.52 and 3.07, and −6.32 kcal/mol and 23.42 μM, respectively, for **2**, **1**, and cisplatin, demonstrating better binding affinity and the smaller amount needed to inhibit the activity of the enzyme. Arg 394, Glu 353, Leu 387, and Leu 391 are the most important active site amino acids of ERα that took part in hydrogen bonding and π-alkyl interactions.[64] The molecular docking analysis results show the involvement of 13 van der Waals and π-alkyl/π-ion type interactions (Met 357, His 356, Ile-386, Leu 387, Gly 390, Phe 445 and Met 357, His 356, Arg 363, Lys 449, Arg 394, Glu 323 and one hydrogen bonding with Trp 393) for **1** and fifteen interactions (Glu 387, Gly 390, Ile 386, His 356, Glu 323, Arg 363 and Arg 394, Lys 449, Pro 406, Glu 353, Leu 403, Ala 405, Leu 349, Trp 360, Met 357) for **2**. On the other hand, cisplatin showed a total of five interactions: two hydrogen bonding (Ser 468, Asp 374), one van der Waals (Lys 467) and two π-alkyl/π-ion (Thr 371, Glu 471) (Table 3). The observed residual amino acid interactions showed that

https://doi.org/10.1021/acsomega.3c00916
ACS Omega 2023, 8, 13421−13434

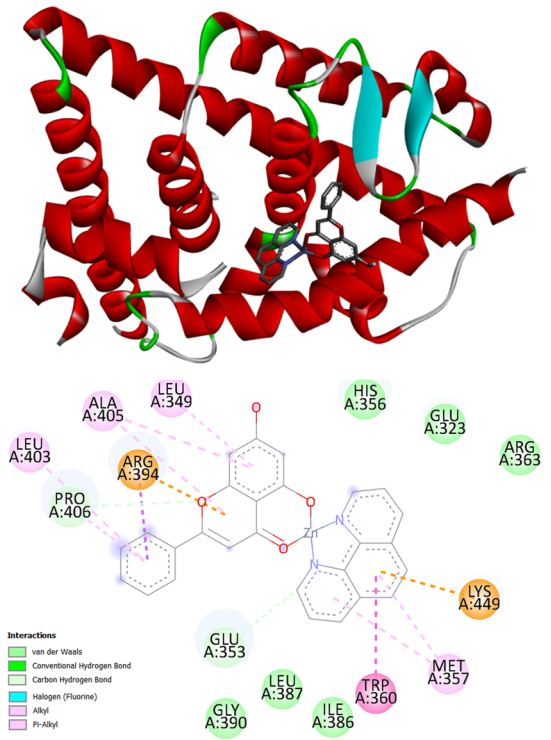

Figure 16. Binding interactions of **2** against estrogen receptor alpha (*ERα*; PDB: 5GS4).

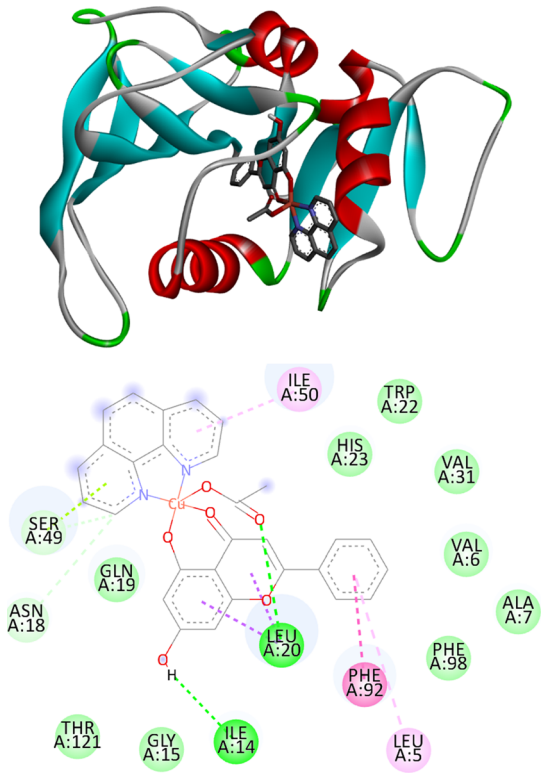

Figure 17. Binding interactions of complex **1** against *S. aureus* (*Dihydrofolate reductase*) (PDB: 2w9h).

the number of interactions affects the binding affinity and K_i of the complexes.

Molecular Docking against *S. aureus*, Dihydrofolate Reductase. Complex **1** established a total of 17 interactions: two hydrogen bonding, Ile 14, Leu 20; 11 van der Walls, Asn 18, Thr 121, Gly 15, Phe 92, Leu 5, Phe 98, Ala 7, Val 6, Val 31, His 23, Trp 22; and four π-alkyl/π-ion, Ile 50, Phe 92, Leu 20, Ser 49 with a binding affinity −7.51 kcal/mol and an inhibition constant of 3.12 μM. In complex **2**, two hydrogen bonding, Leu 20, Gln 19; eight van der Waals, His 23, Asn 18, Thr 46, Gly 94, Ile 14, Gly 93, Lys 52, Ser 49; and five π-alkyl/π-ion, Leu 20, Lys 45, Ser 49, Gln 19, Ile 50 interactions with a binding affinity of −10.75 kcal/mol and an inhibition constant of 0.01 μM, as shown in Figure 17, Table 4, and Figure S5 were observed. The binding affinities of the metal complexes against *dihydrofolate reductase of S. aureus* are in line with the *in vitro* antibacterial percent activity index values of 49.3% for **1** and 39.9% for **2**.

CONCLUSIONS

Chrysin-inspired Cu(II) and Zn(II) complexes employing 1,10-phenathroline co-ligands were synthesized and characterized. DFT, TD-DFT, and molecular docking computational tools were employed to shed more light on the electronic structures of the synthesized metal complexes. Spectroscopic and spectrometric techniques (UV−vis, FTIR, and MS together with TGA/DTA and SEM−EDX) were used to deduce the structures of the reported complexes. Powder XRD results indicated polycrystalline natures of the complexes. The average crystallite sizes of complexes **1** and **2** were 19.766, and 18.050 nm, respectively. On the other hand, percent crystallinity values of 27.208 and 40.914% were found for **1** and **2**, respectively. The molar conductance measurement confirmed the electrolyte nature of complex **2** (51.80 Ω^{-1} mol^{-1} cm^2) and the nonelectrolyte nature of complex **1** (27.56 Ω^{-1} mol^{-1} cm^2). TGA/DTA confirmed the presence of water of crystallization in complex **1**, whereas complex **2** was thermally stable up to 400 °C. These results are consistent with the mass spectrometric findings. Biologically, promising cytotoxicity as well as antibacterial and antioxidant activities were found. The small band gap energy of complex **1** (2.784 eV) from quantum chemical studies showed an association with the percent activity index for the *in vitro* antibacterial activity of complex **1**, ranging from 42.4−49.3% compared to complex **2** (%AI 37.8 to 40.3%). Moreover, Cu(II) complex

Table 3. Molecular Docking Scores and the Corresponding Prominent Residual Amino Acid Interactions of the Complexes against Estrogen Receptor Alpha (ERα; PDB: 5GS4)

cpds	RMSD	binding energy (kcal/mol)	inhibition constant (K_i)	H-bonding	van der Waals	π-alkyl/π-ion
1	0.34	−7.52	3.07 μM	Trp 393	Met 357, His 356, Ile-386, Leu 387, Gly 390, Phe 445	Met 357, His 356, Arg 363, Lys 449, Arg 394, Glu 323
2	0.31	−8.35	0.76 μM		Glu 387, Gly 390, Ile 386, His 356, Glu 323, Arg 363	Arg 394, Lys 449, Pro 406, Glu 353, Leu 403, Ala 405, Leu 349, Trp 360, Met 357
cisplatin	0.39	−6.32	23.42 μM	Ser 468, Asp 374	Lys 467	Thr 371, Glu 471

https://doi.org/10.1021/acsomega.3c00916
ACS Omega 2023, 8, 13421−13434

Table 4. Molecular Docking Scores and the Corresponding Prominent Residual Amino Acid Interactions of the Complexes against *S. aureus* (PDB: 2w9h)

Cpds	RMSD	binding energy (kcal/mol)	inhibition constant (K_i)	H-bonding	van der Waals	π-alkyl/ π-ion
1	0.35	−11.49	0.04 μM	Ile 14, Leu 20	Asn 18, Thr 121, Gly 15, Phe 92, Leu 5, Phe 98, Ala 7, Val 6, Val 31, His 23, Trp 22	Ile 50, Phe 92, Leu 20, Ser 49
2	0.81	−10.75	0.01 μM	Leu 20, Gln 19	His 23, Asn 18, Thr 46, Gly 94, Ile 14, Gly 93, Lys 52, Ser 49	Leu 20, Lys 45, Ser 49, Gln 19, Ile 50
Cipro.	0.92	−8.66	0.45 μM	Asn 18, Asp 27	Lys 45, Ser 49, Thr 46, Leu 28, val 31, Thr 111, Val 6, Leu 5, Phe 98, Gly 94, Ile 14, Gly 13	Ala 17, Leu 20, Thr 46, Ser 49

(**1**) showed significant cytotoxicity against the MCF-7 cell line with an IC_{50} value of 4.09 μM, much less than the standard cisplatin (18.62 μM). The structure−activity relationship also confirmed that complex **1** was 19-fold cytotoxic against the MCF-7 cancer cell line than complex **2**. However, further *in vivo* cytotoxicity studies against the MCF-7 cell lines are recommended.

■ ASSOCIATED CONTENT

Supporting Information

The Supporting Information is available free of charge at https://pubs.acs.org/doi/10.1021/acsomega.3c00916.

Mass spectra of the synthesized complexes; additional molecular docking results; antibacterial activity; quantum chemical descriptors; and optimized geometries of the complexes (PDF)

■ AUTHOR INFORMATION

Corresponding Authors

Mamaru Bitew Alem − *Department of Applied Chemistry, Adama Science and Technology University, Adama 251, Ethiopia;* orcid.org/0000-0002-1880-8572; Email: mamaru2005@gmail.com

Tegene Desalegn − *Department of Applied Chemistry, Adama Science and Technology University, Adama 251, Ethiopia;* orcid.org/0000-0003-0239-8326; Email: tegened@yahoo.com

Taye B. Demissie − *Department of Chemistry, University of Botswana, 0022 Gaborone, Botswana;* orcid.org/0000-0001-8735-4933; Email: demissiet@ub.ac.bw

Authors

Tadewos Damena − *Department of Chemistry, Wachemo University, Hossana 667, Ethiopia;* orcid.org/0000-0001-5345-002X

Enyew Alemayehu Bayle − *Graduate Institute of Applied Science and Technology, National Taiwan University of Science and Technology, 10607 Taipei, Taiwan; Department of Chemistry, Debre Markos University, Debre Markos 269, Ethiopia;* orcid.org/0000-0002-9682-3516

Moses O. Koobotse − *School of Allied Health Professions, University of Botswana, 0022 Gaborone, Botswana*

Kennedy J. Ngwira − *Molecular Sciences Institute, School of Chemistry, University of the Witwatersrand, 2050 Johannesburg, South Africa*

Japheth O. Ombito − *Department of Chemistry, University of Botswana, 0022 Gaborone, Botswana*

Matshediso Zachariah − *School of Allied Health Professions, University of Botswana, 0022 Gaborone, Botswana*

Complete contact information is available at: https://pubs.acs.org/10.1021/acsomega.3c00916

Author Contributions

Experimental: M.B.A., T.D., T.B.D., E.A.B. and M.O.K.; Data analysis: M.B.A., T.D., T.D. and T.B.D.; Methodology: M.B.A., M.O.K., T.D. and T.B.D.; Original draft writing: M.B.A., T.B.D. and T.D.; Writing-review and editing: M.B.A., T.D., T.D., T.B.D., J.O.O., M.O.K., E.A.B., K.J.N. and M.Z.

Notes

The authors declare no competing financial interest.

This study did not include human participants or animals.

■ ACKNOWLEDGMENTS

We would like to acknowledge Adama Science and Technology University and the University of Botswana for technical and material support. Computational resources were supplied by Metacentrum under the project 'e-Infrastructure CZ' (e-INFRA CZ ID: 90140) supported by the Ministry of Education, Youth and Sports of the Czech Republic. We also thank Associate Professor Claire Perks (University of Bristol, United Kingdom) for providing the MCF-7 breast cancer cells, as well as Mosimanegape Baeti and Oarabile Macha for their technical assistance.

■ REFERENCES

(1) (a) Karges, J.; Stokes, R. W.; Cohen, S. M. Metal complexes for therapeutic applications. *Trends Chem.* **2021**, *3*, 523−534. (b) Amarsy, I.; Papot, S.; Gasser, G. Stimuli-Responsive Metal Complexes for Biomedical Applications. *Angew. Chem., Int. Ed.* **2022**, *134*, No. e202205900.

(2) Kilpin, K. J.; Dyson, P. J. Enzyme inhibition by metal complexes: concepts, strategies and applications. *Chem. Sci.* **2013**, *4*, 1410−1419.

(3) Loginova, N. V.; Harbatsevich, H. I.; Osipovich, N. P.; Ksendzova, G. A.; Koval'chuk, T. V.; Polozov, G. I. Metal complexes as promising agents for biomedical applications. *Curr. Med. Chem.* **2020**, *27*, 5213−5249.

(4) Liang, J.; Sun, D.; Yang, Y.; Li, M.; Li, H.; Chen, L. Discovery of metal-based complexes as promising antimicrobial agents. *Eur. J. Med. Chem.* **2021**, *224*, No. 113696.

(5) Renfrew, A. K. Transition metal complexes with bioactive ligands: mechanisms for selective ligand release and applications for drug delivery. *Metallomics* **2014**, *6*, 1324−1335.

(6) Sulpizio, C.; Müller, S. T. R.; Zhang, Q.; Brecker, L.; Rompel, A. Synthesis, characterization, and antioxidant activity of Zn 2+ and Cu 2+ coordinated polyhydroxychalcone complexes. *Monatsh. Chem.* **2016**, *147*, 1871−1881.

(7) (a) Ulas, M.; Orhan, C.; Tuzcu, M.; Ozercan, I. H.; Sahin, N.; Gencoglu, H.; Komorowski, J. R.; Sahin, K. Anti-diabetic potential of chromium histidinate in diabetic retinopathy rats. *BMC Complement Altern. Med.* **2015**, *15*, 16. (b) Peng, M.; Yang, X. Controlling diabetes by chromium complexes: The role of the ligands. *J. Inorg. Biochem.* **2015**, *146*, 97−103.

(8) Kostova, I.; Balkansky, S. Metal complexes of biologically active ligands as potential antioxidants. *Curr. Med. Chem.* **2013**, *20*, 4508−4539.

(9) (a) Zhang, X.; Huang, H.; Zhao, X.; Lv, Q.; Sun, C.; Li, X.; Chen, K. Effects of flavonoids-rich Chinese bayberry (Myrica rubra

Sieb. et Zucc.) pulp extracts on glucose consumption in human HepG2 cells. *J. Funct. Foods* **2015**, *14*, 144−153. (b) AL-Ishaq, R. K.; Abotaleb, M.; Kubatka, P.; Kajo, K.; Büsselberg, D. Flavonoids and their anti-diabetic effects: cellular mechanisms and effects to improve blood sugar levels. *Biomolecules* **2019**, *9*, 430.

(10) (a) Dai, W.; Bi, J.; Li, F.; Wang, S.; Huang, X.; Meng, X.; Sun, B.; Wang, D.; Kong, W.; Jiang; Su, W. Antiviral efficacy of flavonoids against enterovirus 71 infection in vitro and in newborn mice. *Viruses* **2019**, *11*, 625. (b) Xie, Y.; Yang, W.; Tang, F.; Chen, X.; Ren, L. Antibacterial activities of flavonoids: structure-activity relationship and mechanism. *Curr. Med. Chem.* **2015**, *22*, 132−149.

(11) Kasprzak, M. M.; Erxleben, A.; Ochocki, J. Properties and applications of flavonoid metal complexes. *RSC Adv.* **2015**, *5*, 45853−45877.

(12) He, J.-W.; Yang, L.; Mu, Z.-Q.; Zhu, Y.-Y.; Zhong, G.-Y.; Liu, Z.-Y.; Zhou, Q.-G.; Cheng, F. Anti-inflammatory and antioxidant activities of flavonoids from the flowers of Hosta plantaginea. *RSC Adv.* **2018**, *8*, 18175−18179.

(13) Testai, L.; Martelli, A.; Cristofaro, M.; Breschi, M. C.; Calderone, V. Cardioprotective effects of different flavonoids against myocardial ischaemia/reperfusion injury in L angendorff-perfused rat hearts. *J. Pharm. Pharmacol.* **2013**, *65*, 750−756.

(14) Alper, P.; Erkisa, M.; Genckal, H. M.; Sahin, S.; Ulukaya, E.; Ari, F. Synthesis, characterization, anticancer and antioxidant activity of new nickel (II) and copper (II) flavonoid complexes. *J. Mol. Struct.* **2019**, *1196*, 783−792.

(15) Guo, C.; Zhang, H.; Guan, X.; Zhou, Z. The Anti-Aging Potential of Neohesperidin and Its Synergistic Effects with Other Citrus Flavonoids in Extending Chronological Lifespan of Saccharomyces Cerevisiae BY4742. *Molecules* **2019**, *24*, 4093.

(16) (a) Krych, J.; Gebicka, L. Catalase is inhibited by flavonoids. *Int. J. Biol. Macromol.* **2013**, *58*, 148−153. (b) Ayaz, M.; Sadiq, A.; Junaid, M.; Ullah, F.; Ovais, M.; Ullah, I.; Ahmed, J.; Shahid, M. Flavonoids as prospective neuroprotectants and their therapeutic propensity in aging associated neurological disorders. *Front. Aging Neurosci.* **2019**, *11*, 155.

(17) Ragab, F.; Yahya, T.; El-Naa, M.; Arafa, R. Design, synthesis and structure−activity relationship of novel semi-synthetic flavonoids as antiproliferative agents. *Eur. J. Med. Chem.* **2014**, *82*, 506−520.

(18) (a) Collins-Burow, B. M.; Antoon, J. W.; Frigo, D. E.; Elliott, S.; Weldon, C. B.; Boue, S. M.; Beckman, B. S.; Curiel, T. J.; Alam, J.; McLachlan, J. A.; Burow, M. E. Antiestrogenic activity of flavonoid phytochemicals mediated via the c-Jun N-terminal protein kinase pathway. Cell-type specific regulation of estrogen receptor alpha. *J. Steroid Biochem. Mol. Biol.* **2012**, *132*, 186−193. (b) Collins-Burow, B. M.; Burow, M. E.; Duong, B. N.; McLachlan, J. A. Estrogenic and antiestrogenic activities of flavonoidphytochemicals through estrogen receptorbinding-dependent and-independent mechanisms. *Nutr. Cancer* **2000**, *38*, 229−244.

(19) Vinayagam, R.; Xu, B. Antidiabetic properties of dietary flavonoids: a cellular mechanism review. *Nutr. Metab.* **2015**, *12*, 60.

(20) Atabey-Ozdemir, B.; Demirkiran, O.; Yildiz, U.; Tekin, I.; Coban, B. Cytotoxicity and DNA binding of copper (II) and zinc (II) complexes of flavonoids: quercitrin, myricitrin, rutin. *Bulg. Chem. Commun.* **2017**, *49*, 901−907.

(21) Bitew, M.; Desalegn, T.; Demissie, T. B.; Belayneh, A.; Endale, M.; Eswaramoorthy, R. Pharmacokinetics and drug-likeness of antidiabetic flavonoids: Molecular docking and DFT study. *PLoS One* **2021**, *16*, No. e0260853.

(22) (a) Spoerlein, C.; Mahal, K.; Schmidt, H.; Schobert, R. Effects of chrysin, apigenin, genistein and their homoleptic copper (II) complexes on the growth and metastatic potential of cancer cells. *J. Inorg. Biochem.* **2013**, *127*, 107−115. (b) Halevas, E.; Mavroidi, B.; Antonoglou, O.; Hatzidimitriou, A.; Sagnou, M.; Pantazaki, A. A.; Litsardakis, G.; Pelecanou, M. Structurally characterized gallium−chrysin complexes with anticancer potential. *J. Chem. Soc., Dalton Trans.* **2020**, *49*, 2734−2746. (c) Nandanwar, S. K.; Kim, H. J. Anticancer and antibacterial activity of transition metal complexes. *ChemistrySelect* **2019**, *4*, 1706−1721.

(23) Lin, S.; Zeng, L.; Zhang, G.; Liao, Y.; Gong, D. Synthesis, characterization and xanthine oxidase inhibition of Cu (II)−chrysin complex. *Spectrochim. Acta A Mol. Biomol. Spectrosc.* **2017**, *178*, 71−78.

(24) Halevas, E.; Mavroidi, B.; Pelecanou, M.; Hatzidimitriou, A. G. Structurally characterized zinc complexes of flavonoids chrysin and quercetin with antioxidant potential. *Inorg. Chim. Acta* **2021**, *523*, No. 120407.

(25) Gençkal, H. M. New heteroleptic Cu (II) complexes of chrysin with 2, 2′−bipyridine and substituted 1, 10−phenanthrolines: Synthesis, characterization, thermal stability and antioxidant activity. *J. Mol. Struct.* **2020**, *1209*, No. 127917.

(26) Halevas, E.; Mitrakas, A.; Mavroidi, B.; Athanasiou, D.; Gkika, P.; Antoniou, K.; Samaras, G.; Lialiaris, E.; Hatzidimitriou, A.; Pantazaki, A.; Koukourakis, M.; Sagnou, M.; Pelecanou, M.; Lialiaris, T. Structurally characterized copper-chrysin complexes display genotoxic and cytotoxic activity in human cells. *Inorg. Chim. Acta* **2021**, *515*, No. 120062.

(27) Alem, M.; Damena, T.; Desalegn, T.; Koobotse, M.; Eswaramoorthy, R.; Ngwira, K.; Ombito, J.; Zachariah, M.; Demissie, T. Cytotoxic mixed-ligand complexes of Cu (II): A combined experimental and computational study. *Front. Chem.* **2022**, *10*, No. 1028957.

(28) Holzwarth, U.; Gibson, N. The Scherrer equation versus the'Debye-Scherrer equation'. *Nat. Nanotechnol.* **2011**, *6*, 534−534.

(29) Altomare, A.; Corriero, N.; Cuocci, C.; Falcicchio, A.; Moliterni, A.; Rizzi, R. QUALX2. 0: a qualitative phase analysis software using the freely available database POW_COD. *J. Appl. Crystallogr.* **2015**, *48*, 598−603.

(30) Ommenya, F. K.; Nyawade, E. A.; Andala, D. M.; Kinyua, J. Synthesis, characterization and antibacterial activity of Schiff base, 4-Chloro-2-{(E)-[(4-fluorophenyl) imino] methyl} phenol metal (II) complexes. *J. Chem.* **2020**, *2020*, 1−8.

(31) Gulcin, İ. Antioxidants and antioxidant methods: An updated overview. *Arch. Toxicol.* **2020**, *94*, 651−715.

(32) (a) Beck, A. D. Density-functional thermochemistry. III. The role of exact exchange. *J. Chem. Phys.* **1993**, *98*, 5648−5652. (b) Lee, C.; Yang, W.; Parr, R. G. Development of the Colle-Salvetti correlation-energy formula into a functional of the electron density. *Phys. Rev. B* **1988**, *37*, 785. (c) Stephens, P. J.; Devlin, F. J.; Chabalowski, C. F.; Frisch, M. J. Ab initio calculation of vibrational absorption and circular dichroism spectra using density functional force fields. *J. Phys. Chem.* **1994**, *98*, 11623−11627.

(33) Krishnan, R.; Binkley, J. S.; Seeger, R.; Pople, J. A. Self-consistent molecular orbital methods. XX. A basis set for correlated wave functions. *J. Chem. Phys.* **1980**, *72*, 650−654.

(34) Hay, P. J.; Wadt, W. R. Ab initio effective core potentials for molecular calculations. Potentials for the transition metal atoms Sc to Hg. *J. Chem. Phys.* **1985**, *82*, 270−283.

(35) Grimme, S.; Furche, F.; Ahlrichs, R. An improved method for density functional calculations of the frequency-dependent optical rotation. *Chem. Phys. Lett.* **2002**, *361*, 321−328.

(36) Demissie, T. B.; Hansen, J. H. Mechanism and site selectivity in visible-light photocatalyzed C−H functionalization: insights from DFT calculations. *J. Org. Chem.* **2016**, *81*, 7110−7120.

(37) Pratiwi, R.; Ibrahim, S.; Tjahjono, D. H. Reactivity and Stability of Metalloporphyrin Complex Formation: DFT and Experimental Study. *Molecules* **2020**, *25*, 4221.

(38) Ismael, M.; Abdel-Mawgoud, A.-M. M.; Rabia, M. K.; Abdou, A. Design and synthesis of three Fe (III) mixed-ligand complexes: Exploration of their biological and phenoxazinone synthase-like activities. *Inorg. Chim. Acta* **2020**, *505*, No. 119443.

(39) Xie, M.; Zhao, H.; Liu, Q.; Zhu, Y.; Yin, F.; Liang, Y.; Jiang, Y.; Wang, D.; Hu, K.; Qin, X.; et al. Structural Basis of Inhibition of ERα-Coactivator Interaction by High-Affinity N-Terminus Isoaspartic Acid Tethered Helical Peptides. *J. Med. Chem.* **2017**, *60*, 8731−8740.

(40) Allouche, A. R. Gabedit—A graphical user interface for computational chemistry softwares. *Comput. Chem.* **2011**, *32*, 174−182.

https://doi.org/10.1021/acsomega.3c00916
ACS Omega 2023, 8, 13421−13434

(41) Lemilemu, F.; Bitew, M.; Demissie, T. B.; Eswaramoorthy, R.; Endale, M. Synthesis, antibacterial and antioxidant activities of Thiazole-based Schiff base derivatives: a combined experimental and computational study. *BMC Chem.* **2021**, *15*, 67.
(42) Morris, G. M.; Goodsell, D. S.; Halliday, R. S.; Huey, R.; Hart, W. E.; Belew, R. K.; Olson, A. J. Automated docking using a Lamarckian genetic algorithm and an empirical binding free energy function. *J. Comput. Chem.* **1998**, *19*, 1639−1662.
(43) Ördög, R.; Grolmusz, V. Evaluating genetic algorithms in protein-ligand docking. In *Int. J. Bioinform. Res. Appl.*; Springer: 2008, 402−413.
(44) Ali, I.; Wani, W. A.; Saleem, K. Empirical formulae to molecular structures of metal complexes by molar conductance. *Synth. React. Inorg. Met.-Org. Nano-Met. Chem.* **2013**, *43*, 1162−1170.
(45) Karabacak, M.; Cinar, Z.; Kurt, M.; Sudha, S.; Sundaraganesan, N. FT-IR, FT-Raman, NMR and UV−vis spectra, vibrational assignments and DFT calculations of 4-butyl benzoic acid. *Spectrochim. Acta A Mol. Biomol. Spectrosc.* **2012**, *85*, 179−189.
(46) Abebe, A.; Bayeh, Y.; Belay, M.; Gebretsadik, T.; Thomas, M.; Linert, W. Mono and binuclear cobalt (II) mixed ligand complexes containing 1, 10-phenanthroline and adenine using 1, 3-diaminopropane as a spacer: synthesis, characterization, and antibacterial activity investigations. *Futur. J. Pharm. Sci.* **2020**, *6*, 13.
(47) Dehghan, G.; Khoshkam, Z. Tin (II)−quercetin complex: Synthesis, spectral characterisation and antioxidant activity. *Food Chem.* **2012**, *131*, 422−426.
(48) Panhwar, Q. K.; Memon, S. Synthesis of Cr (III)-morin complex: Characterization and antioxidant study. *ScientificWorldJournal* **2014**, *2014*, No. 845208.
(49) Damena, T.; Alem, M. B.; Zeleke, D.; Desalegn, T.; Eswaramoorthy, R.; Demissie, T. B. Synthesis, characterization, and biological activities of zinc (II), copper (II) and nickel (II) complexes of an aminoquinoline derivative. *Front. Chem.* **2022**, *10*, No. 1053532.
(50) Lawal, M.; Obaleye, J. A.; Jadeja, R. N.; Bamigboye, M. O.; Gupta, V. K.; Roy, H.; Shaikh, I. U. Copper (II) mixed-ligand complexes with fluoroquinolones and an N-donor co-ligand: Structures and biological application. *Polyhedron* **2020**, *190*, No. 114753.
(51) El-Sonbati, A. Z.; Diab, M. A.; Eldesoky, A. M.; Morgan, S. M.; Salem, O. L. Polymer complexes. LXXVI. Synthesis, characterization, CT-DNA binding, molecular docking and thermal studies of sulfoxine polymer complexes. *Appl. Organomet. Chem.* **2019**, *33*, No. e4839.
(52) El-Sonbati, A.; Omar, N.; Abou-Dobara, M.; Diab, M.; El-Mogazy, M.; Morgan, S. M.; Hussien, M.; El-Ghettany, A. Structural, molecular docking computational studies and in-vitro evidence for antibacterial activity of mixed ligand complexes. *J. Mol. Struct.* **2021**, *1239*, No. 130481.
(53) (a) Abbas, B. F.; Kamel, B. A. F.; Khamais, W. M. Preparation, diagnosis, biological activity, and theoretical studies of some mixed drug complexes. *ScientificWorldJournal* **2019**, *2019*, No. 8962923. (b) Abd El-Halim, H. F.; Mohamed, G. G.; Khalil, E. A. Synthesis, spectral, thermal and biological studies of mixed ligand complexes with newly prepared Schiff base and 1, 10-phenanthroline ligands. *J. Mol. Struct.* **2017**, *1146*, 153−163.
(54) Bravo-Gómez, M. E.; García-Ramos, J. C.; Gracia-Mora, I.; Ruiz-Azuara, L. Antiproliferative activity and QSAR study of copper (II) mixed chelate [Cu (N−N)(acetylacetonato)] NO3 and [Cu (N−N)(glycinato)] NO3 complexes,(Casiopeínas). *J. Inorg. Biochem.* **2009**, *103*, 299−309.
(55) Nunes, P.; Correia, I.; Marques, F.; Matos, A. P.; Dos Santos, M. M.; Azevedo, C. G.; Capelo, J.-L.; Santos, H. M.; Gama, S.; Pinheiro, T. Copper complexes with 1, 10-phenanthroline derivatives: underlying factors affecting their cytotoxicity. *Inorg. Chem.* **2020**, *59*, 9116−9134.
(56) (a) Cannella, V.; Altomare, R.; Chiaramonte, G.; Di Bella, S.; Mira, F.; Russotto, L.; Pisano, P.; Guercio, A. Cytotoxicity evaluation of endodontic pins on L929 cell line. *Biomed Res. Int.* **2019**, *2019*, No. 3469525. (b) Ramasamy, S.; Muthusamy, S.; Nagarajan, S.; Nath, A. V.; Savarimuthu, J. S.; Jayaprakash, J.; Gurunadhan, R. M. Fabrication of collagen with polyhexamethylene biguanide: A potential scaffold for infected wounds. *J. Biomed. Mater. Res.* **2022**, *110*, 535−546. (c) Roth, R.; Coemert, S.; Burkhardt, S.; Rodewald, K. S.; Lueth, T. C. A process towards eliminating cytotoxicity by removal of surface contamination from electrical discharge machined nitinol. *Procedia CIRP* **2020**, *89*, 45−51.
(57) (a) Andiappan, K.; Sanmugam, A.; Deivanayagam, E.; Karuppasamy, K.; Kim, H.-S.; Vikraman, D. In vitro cytotoxicity activity of novel Schiff base ligand−lanthanide complexes. *Sci. Rep.* **2018**, *8*, 3054. (b) Razak, N. A.; Abu, N.; Ho, W. Y.; Zamberi, N. R.; Tan, S. W.; Alitheen, N. B.; Long, K.; Yeap, S. K. Cytotoxicity of eupatorin in MCF-7 and MDA-MB-231 human breast cancer cells via cell cycle arrest, anti-angiogenesis and induction of apoptosis. *Sci. Rep.* **2019**, *9*, 1514.
(58) Damena, T.; Alem, M. B.; Zeleke, D.; Demissie, T. B.; Desalegn, T. Synthesis and Computational Studies of Novel Cobalt (II) and Oxovanadium (IV) Complexes of Quinoline Carbaldehyde Derivative Ligand for Antibacterial and Antioxidant Applications. *J. Mol. Struct.* **2023**, *1280*, No. 134994.
(59) LoPachin, R. M.; Gavin, T.; DeCaprio, A.; Barber, D. S. Application of the hard and soft, acids and bases (HSAB) theory to toxicant−target interactions. *Chem. Res. Toxicol.* **2012**, *25*, 239−251.
(60) LoPachin, R. M.; Gavin, T. Molecular mechanisms of aldehyde toxicity: a chemical perspective. *Chem. Res. Toxicol.* **2014**, *27*, 1081−1091.
(61) Rahmouni, N. T.; el Houda Bensiradj, N.; Megatli, S. A.; Djebbar, S.; Baitich, O. B. New mixed amino acids complexes of iron (III) and zinc (II) with isonitrosoacetophenone: Synthesis, spectral characterization, DFT study and anticancer activity. *Spectrochim. Acta A Mol. Biomol. Spectrosc.* **2019**, *213*, 235−248.
(62) Ferchichi, A.; Makhlouf, J.; El Bakri, Y.; Saravanan, K.; Valkonen, A.; Hashem, H. E.; Ahmad, S.; Smirani, W. Self-assembly of new cobalt complexes based on [Co (SCN) 4], synthesis, empirical, antioxidant activity, and quantum theory investigations. *Sci. Rep.* **2022**, *12*, 15828.
(63) Bhatt, S.; Stender, J. D.; Joshi, S.; Wu, G.; Katzenellenbogen, B. S. OCT-4: a novel estrogen receptor-α collaborator that promotes tamoxifen resistance in breast cancer cells. *Oncogene* **2016**, *35*, 5722−5734.
(64) Pang, X.; Fu, W.; Wang, J.; Kang, D.; Xu, L.; Zhao, Y.; Liu, A.-L.; Du, G.-H. Identification of estrogen receptor α antagonists from natural products via in vitro and in silico approaches. *Oxid. Med. Cell. Longev.* **2018**, *2018*, No. 6040149.

https://doi.org/10.1021/acsomega.3c00916
ACS Omega 2023, 8, 13421−13434